Line-field confocal optical coherence tomography operating simultaneously at 800 nm and 1300 nm center wavelengths

Arthur Davis, Olivier Levecq, Hicham Azimani, David Siret, Arnaud Dubois

Line-field confocal optical coherence tomography operating simultaneously at 800 nm and 1300 nm center wavelengths

Arthur Davis[a,b], Olivier Levecq[a], Hicham Azimani[a], David Siret[a], Arnaud Dubois[a,b]
[a]DAMAE Medical, 28 rue de Turbigo, 75003 Paris, France; [b]Laboratoire Charles Fabry, Institut d'Optique Graduate School, Université Paris-Saclay, 91127 Palaiseau Cedex, France

ABSTRACT

An imaging device based on line-field confocal optical coherence tomography (LC-OCT) operating in two distinct spectral bands centered at 770 nm and 1250 nm is presented. A single supercontinuum light source and two different line-scan cameras are used. B-scans are acquired simultaneously in the two bands at 4 frames per second. In the 770-nm band, high resolution (1.3 µm x 1.2 µm, lateral x axial) imaging is achieved, while extended penetration (~ 700 µm) is obtained in the 1250-nm band. Greyscale fusion of the two images is performed to produce a single image with both high resolution in the superficial part of the image and deep penetration. A color representation is also used to highlight spectroscopic properties of the sample and to enhance contrast.

Keywords: Optical coherence tomography, medical and biological imaging, interference microscopy.

1. INTRODUCTION

First proposed in 1991, optical coherence tomography (OCT) is an imaging method based on low-coherence interferometry for semi-transparent samples imaging with spatial resolution between 1 and 15 µm [1]. OCT has rapidly proved itself to be a valuable tool in the field of medical imaging [2], in particular in ophthalmology [3]. It has also been used in cardiology [4], gastroenterology [5], and dermatology [6].

Line-field confocal optical coherence tomography (LC-OCT) is a recently invented optical imaging device based on time-domain OCT [7]. Using line illumination and detection, multiple A-scans are acquired in parallel to form a B-scan. Thus, a single axial scan is required to reproduce a complete image. During the scan, the focus of the microscope objective is continuously adjusted, allowing the use of relatively high numerical apertures (NA), thus improving the lateral resolution compared to conventional OCT systems. A supercontinuum laser is used as a temporally incoherent light source and the optical dispersion between the arms of the interferometer is balanced in order to reach the best axial resolution in OCT images at similar wavelengths [8,9]. Line illumination and detection provide an efficient confocal gate rejecting most of the out-of-focus light that does not contribute to the signal, thus allowing to image deep in biological samples [10]. A silicon-based CCD camera is used to detect the backscattered signal. The contributions of the emission spectrum of the laser and the detection spectrum camera result in a detected spectrum centered at ~ 800 nm with a spatial resolution of ~ 1 µm in both directions [11]. The imaging penetration depth in skin is ~ 400 µm, allowing to see clearly the dermo-epidermal junction (DEJ) where most tumors appear. This device is therefore particularly adapted to skin cancer detection, especially melanoma. However, the imaging depth might be an obstacle for certain applications such as the evaluation of margins during Mohs surgery, or the investigation of collagen fibers in dermo-cosmetics.

Scattering is the limiting factor of penetration depth in most biological tissues [12], and its efficiency decreases with the wavelength. Therefore, imaging at higher wavelengths can substantially improve the penetration depth if absorption does not become limiting [13]. It has been demonstrated that the 1300-nm band is optimal for penetration [14]. However, spatial resolution also depends on the wavelength, resulting in a compromise between resolution and penetration. It is then interesting to work with two different spectral bands in order to benefit from the specific advantages of each band [15–18].

In this paper we present a device coupling together two LC-OCT systems to image simultaneously in two distinct spectral bands: one centered around 770 nm called the VIS/nIR band producing high resolution images, the other one centered around 1250 nm called the nIR band producing images with extended depth penetration. Greyscale fusion is

performed to produce a single greyscale image retaining the best of both images. Finally, the contrast of the images is enhanced and spectroscopic information highlighted by a color representation of the two images.

2. EXPERIMENTAL SETUP

The diagram of our dual-band LC-OCT system is represented in Fig. 1. The core of the prototype is a Linnik-type interferometer composed of a non-polarizing beam-splitter and two identical water-immersion microscope objectives (Olympus UMPLanFLN 20x/0.5 W). Both microscope objectives are placed on a piezoelectric-driven linear stage (Physik Instrumente P625.1CD). The objective in the reference arm is translated to displace the coherence plane, *i.e.* the plane of zero optical path difference, in order to scan the sample in depth, while the position of the objective in the sample arm is moved to adjust the focus. The beam-splitter is designed with antireflection and beam-splitter coatings for the band between 1100 nm and 1600 nm. The broadband light source is a supercontinuum laser (NKT Photonics SuperK EXR4) which has an emission spectrum ranging from 480 nm to 2100 nm with a maximum total power of 2 W. The collimated beam from the light source is shaped in the form of a line of light by a 50-mm cylindrical lens. The backscattered signal collected from the sample microscope objective is then focused using two different 200-mm tube lenses after spectral separation by a long-pass dichroic mirror with a cutoff wavelength of 950 nm (Thorlabs DMLP950). Two different line scan cameras are used to detect the signal: a silicon CCD camera (Teledyne-e2V Aviiva EM4 BA9, 2048 pixels, 12 bits, 70 kHz) with 14 µm × 28 µm pixels (width × height) for the VIS/nIR band, and an InGaAs camera (SUI Goodrich LDH2, 1024 pixels, 12 bits, 91 kHz) with 25-µm square pixels for the nIR band.

Chromatic aberrations in the microscope objectives result in a focus gap of 20 µm between the two bands in the object. Schematically, there are two distinct focus planes associated with each of the two bands, whereas the coherence plane is unique as it does not depend on the wavelength if optical dispersion mismatch in the interferometer arms is negligible. The focus gap being greater than the depth of focus of the microscope objectives, it is impossible to simultaneously superimpose the coherence plane with the two focal planes. The first step to adjust the prototype is to adapt the optical path in the reference arm in order to match the objective's focal plane in the VIS/nIR band. The Si camera is placed at the focal plane of tube lens L3 so that it is conjugated with the focal plane of the objective, and thus with the coherence plane. The InGaAs camera is transposed 11 mm away from the focal plane of tube lens L2 to be conjugated with the VIS/nIR focal plane in the object space. The microscope objective and the tube lens in the nIR band are not working in their optimal configuration, but no degradation in image resolution could be detected compared to the ideal conjugation.

The illumination beam must also be focused in the coherence plane for both bands, which cannot be done using a single illumination because of chromatic aberrations of the microscope objectives. The beam from the supercontinuum laser is brought to the optical set-up by a photonic crystal fiber where the supercontinuum generation occurs. The beam is then spectrally divided by a dichroic mirror with a cutoff wavelength of 950 nm (NKT SuperK Split). The two resulting beams are injected in adapted single mode fibers and collimated using off-axis parabolas (Thorlabs RC12APC-P01 for the VIS/nIR band; Thorlabs RC08APC-P01 for the nIR band). In the path of the nIR beam is inserted an optical system with an adjustable focal length, which is in practice a fixed magnification beam expander with an adjustable collimation (Thorlabs GBE02-C), in order to superimpose the nIR illumination line with the VIS/nIR line in the sample. A long-pass filter at 1100 nm is also placed in the path of the nIR illumination beam to block the high peak at 1064 nm of the supercontinuum laser. The beams are finally recombined using a long-pass dichroic mirror (Thorlabs DMLP950).

The microscope objectives are immerged in vats sealed with a 500-µm thick fused silica glass plate and filled with an immersion liquid (Cargille Laboratories, n = 1.4035 at 583.3 nm) transparent in both bands and with an optical index matching the mean optical index of skin. The index matching ensures that the focal plane and the coherence plane remain superimposed when imaging in depth [19]. In the reference arm, the interface between the external side of the glass plate and air serves as a reference surface reflecting 3-4 % of light in the VIS/nIR and nIR bands respectively. In the sample arm, the glass plate is used for equalizing the optical dispersion between the two arms of the interferometer and offers a flat and stable contact surface for the samples. A dermoscopic oil is used to ensure the optical contact between the sample and the glass plate.

The amplitude of the interferometric signal acquired by the cameras during the scan of the sample is extracted numerically by using a five-frame phase-shifting algorithm with a phase step of $\pi/2$ [20]. The displacement of the coherence plane within the sample creates a phase shift between successive frames. For a phase shift of $\pi/2$, the

displacement should be $\delta z = \lambda_0 / 8n$ where λ_0 is the central wavelength of the detected spectrum and n the optical index of the immersion medium. The required displacements are 68.8 nm and 113.2 nm and the VIS/nIR and nIR bands respectively. The cameras are then triggered timewise with appropriate frequencies to ensure the correct phase shift between successive images. For 700 µm-deep B-scans at 4 frames per second, the triggering frequencies are respectively 46.5 kHz and 26.5 kHz for the Si camera and the InGaAs camera. The images acquired by the cameras are transferred to a control unit where they are scaled and processed before display on a computer monitor with a gamma correction factor of 0.25 in each band.

To compare the images acquired in both bands, they must have the same field of view. The Si camera has 2048 14-µm pixels (total width of 28.7 mm) while the InGaAs detector has 1024 25-µm pixels (total width of 25.6 mm). An initial step of registration is therefore necessary to make the two images coincide in the object space. For this purpose, a reference object composed of thin glass plates arranged in the form of "stairs" is imaged. A transformation is computed using points common in both images, which are distinguishable thanks to the edges of the reference object. Distances are then equivalent in both images. Finally, the VIS/nIR is cropped on the sides so that both images display the same field of view. In the object space, the dimensions of the images are 1.15 mm x 0.7 mm (width x depth).

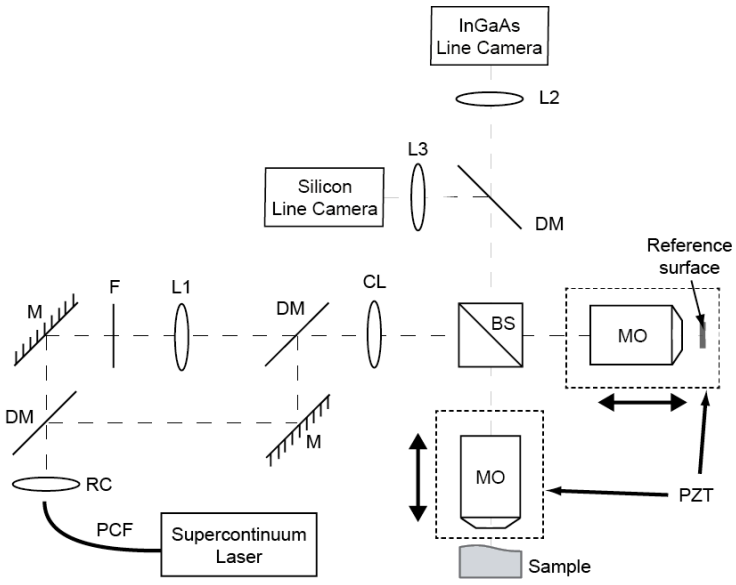

Fig. 1. Diagram of the dual-band LC-OCT prototype. PCF: photonic-crystal fiber; RC: reflective collimator; DM: long-pass (950 nm) dichroic mirror; F: long-pass filter; M: mirror; L1: adjustable focal length optical system; CL: cylindrical lens; BS: cube beam-splitter; MO: microscope objective; PZT: piezoelectric linear stage; L2, L3: tube lenses.

3. SYSTEM CHARACTERIZATION

In order to characterize the system, the spectral bands we measured through a Fourier analysis of the interference pattern acquired with a glass/air interface as the object. The measured spectra are the result of the contribution of the emission spectrum of the light source, the detection spectra of the cameras, and the transmission/reflectivity of all the optical components of the system. Before detection, the spectrum is divided by a long-pass dichroic mirror with a cutoff wavelength of 950 nm. A long-pass filter with a cutoff wavelength of 1100 nm is placed in the nIR detection path to remove the high peak in the supercontinuum laser spectrum at 1064 nm. This is necessary to avoid strong side lobes in the axial response to would generate artifacts in the image. The center wavelength is defined as the center of mass of the spectrum, while the spectral width $\Delta\lambda$ is derived from the variance σ_λ of the spectral distribution: $\Delta\lambda = 2\sqrt{2\ln 2}\,\sigma_\lambda$. According to these definitions, center wavelengths of 770 nm and 1250 nm are measured for the VIS/nIR band and the nIR band respectively. The spectral widths are 150 nm and 210 nm respectively.

The axial resolution of the imaging system is defined as the full width at half maximum (FWHM) of the envelop of the interference pattern. The method presented in [21] is used to flatten the interference pattern to remove the confocal reflection and to extract the envelop of the fringes. Axial resolutions of 1.2 µm and 2.7 µm are measured in the VIS/nIR band and the nIR band respectively. Theoretical axial resolutions can be computed assuming gaussian-shaped spectra. They are 1.3 µm and 2.4 µm respectively. The disagreement between the experimental and theoretical values is partially caused by the non-gaussian shape of the spectra. Besides, a slight dispersion mismatch between the two arms of the interferometer may also degrade the experimental value. As for the VIS/nIR experimental value which seems to be better than the theoretical one, this is attributed to the presence of non-negligible side lobes in the interference pattern that lead to an optimistic value of the resolution using the FWHM definition.

The transverse resolution of our system is defined as the 20-80% width of the profile in intensity of an object presenting a sharp edge. They are measured at 1.3 µm and 2.3 µm in the VIS/nIR band and the nIR band respectively. Compared to the transverse resolution of a diffraction-limited imaging system, the experimental results are about 40 % larger than the theoretical values in both bands. Optical aberrations resulting from the use of a different immersion medium than water and the presence of a 500-µm thick glass plate could explain this degradation. However, the measured values are consistent with the central wavelengths since the ratio of the transverse resolutions is approximately equal to the ratio of the central wavelengths.

In LC-OCT, axial and transverse resolutions are uncorrelated, meaning that it is possible to obtain quasi-isotropic spatial resolution without the need of very high numerical aperture objectives. It is worth noting that the spatial resolution is measured at the surface. It is fairly possible that certain phenomena such as optical aberrations and dispersion mismatch between the two arms of the interferometer may degrade the resolution in depth. However, we used microscope objectives with a moderate numerical aperture of 0.5, so that the beam is little affected by passing through turbid media such as skin. Besides, the optical index of the immersion medium is close to that of the skin to minimize dispersion mismatch. Consequently, we can reasonably assume that the degradation of the resolution is limited when imaging at depths less than several hundreds of micrometers. This assumption seems to be confirmed by the observation of the images.

Detection sensitivity is defined as the minimal detectable reflectivity. In practice, it is considered to be the mean value of the background noise of the images. By placing an object of known reflectivity in the image it is possible to express the measured value as an equivalent reflectivity. For this purpose, an object formed by the interface between glass and a dermoscopic oil reflecting ~ 8×10^{-5} was used to calibrate the measurement. The detection sensitivity was measured at 86 dB and 94 dB in the VIS/nIR band and the nIR band respectively. The gap between the two bands can mainly be explained by the difference between the full well capacities of the detectors (0.31 Me- for the Si camera, 8.7 Me- for the InGaAs camera). However, if the full well capacity could explain the difference entirely, the gap should be of 14.4 dB. Experimentally, the difference is lower because the InGaAs camera is not shot-noise limited [22].

4. APPLICATION TO SKIN IMAGING

In Fig. 2 are displayed images of human skin (25-year old male, back of the hand) acquired in the two bands simultaneously. In both bands, penetration is sufficient to see the two most superficial layers of the skin: the epidermis and the dermis. The epidermis can be divided in several sublayers: the stratum corneum, the stratum granulosum, the stratum spinosum, and the basal layer. As for the dermis, it is mostly composed of collagen fibers, blood vessels, and scattered cells. The VIS/nIR image (a) displays high resolution in the superficial parts of the skin but a penetration limited to ~ 400 µm. The nIR images (b) penetrate deeper (~ 700 µm), allowing seeing much deeper into the dermis, at the cost of a degradation of the spatial resolution. The reduction in spatial resolution is quite clear in Fig. 2 (e) and (f) when looking at the epidermis where the cell nuclei are less noticeable.

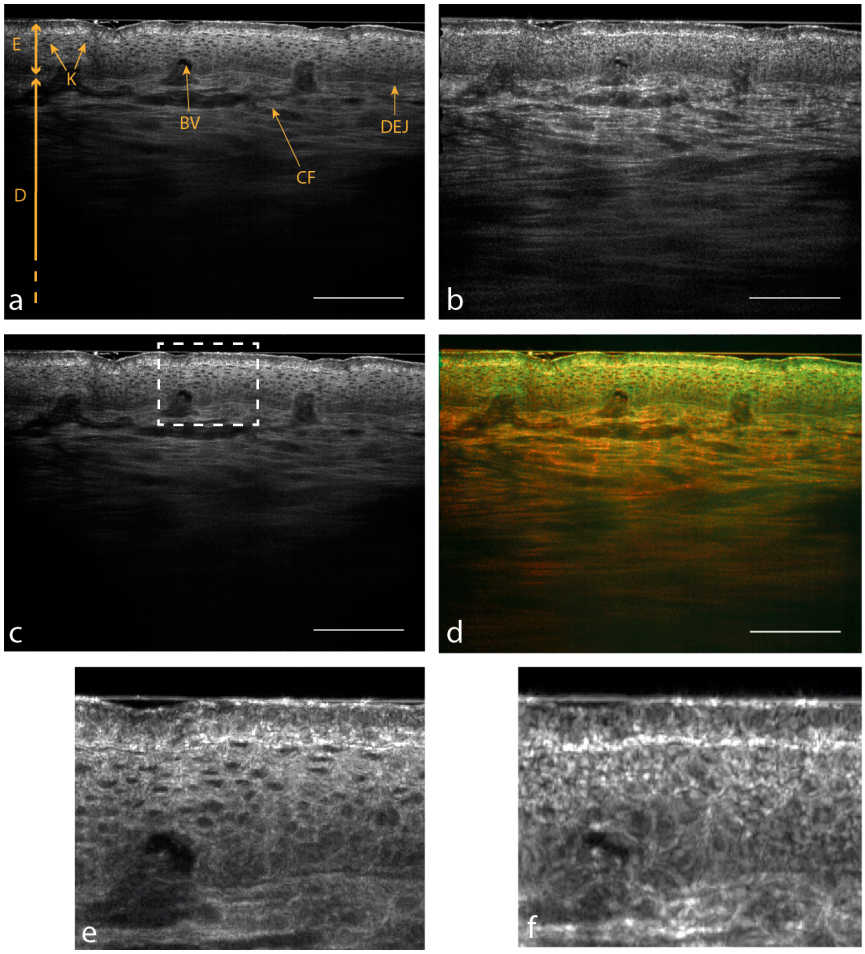

Fig. 2. *In vivo* B-scans of the back of the hand acquired simultaneously in the VIS/nIR band centered at 770 nm (a) and in the nIR band centered at 1250 nm (b). (c) Compounded image from (a) and (b) using a greyscale "up-down" fusion law. (d) Color representation of (a) assigned to the green channel and (b) to the red channel. (e) and (f) are magnified images from (a) and (b) respectively, corresponding to the region in the dashed frame drawn in (c). Scale bar: 200 µm.

Greyscale fusion of the images acquired in both bands is performed using an "up-down" method. A higher weight is attributed in the superficial part of the VIS/nIR image whereas a higher weight is attributed to the nIR image in depth. The result is a single greyscale image combining the valuable features of both bands. This method was used to create the compounded image, shown in Fig. 2(c), which displays high resolution in the epidermis and high penetration in the dermis. Another advantage of the greyscale compounding is that, since the output is the result of a linear combination of the images, speckle noise can be reduced to some extent through frequency compounding [23,24]. It should be noted that speckle noise can effectively be reduced with a simple temporal average of successive images through spatial compounding thanks to the micro-movements of the sample during the acquisition time.

Color fusion was also performed to enhance image contrast and to reveal spectroscopic information about the sample. Indeed, using a color representation in the red-green-blue color space, areas predominant in either band can be highlighted. The image shown in Fig. 2(d) is the result of assigning the nIR image to the red channel and the VIS/nIR image to the green channel. Consequently, areas scattering mostly in the nIR band appear in red, while areas scattering mostly in the VIS/nIR band are shown in green. Areas where scattering in the VIS/nIR band and in the nIR band are equivalent appear in yellowish tones. In the absence of scattering the pixel is black. With this method, the brightness of a pixel depends on the intensities of the individual images. Therefore, the color image is in terms of intensity equivalent to an average pixel per pixel of the individual images. In the resulting image, the epidermis appears mainly yellow because

both bands are equally prominent, while the dermis has a color gradient from orange to red in accordance with the reduction in scattering efficiency as the wavelength becomes longer.

5. CONCLUSION

LC-OCT is an imaging method capable of overcoming the lack of resolution of conventional OCT. Thanks to line illumination coupled with line detection, A-scans are acquired in parallel. B-scans are reconstituted in a single axial scan, which allows the use of high NA microscope objectives and their dynamic focusing. Most of the incoherent light is effectively rejected by a line confocal gating, thus improving the penetration in images while preserving an acquisition speed allowing real-time and *in vivo* imaging. However, when designing an LC-OCT system, we are compelled to make a compromise between resolution and penetration by choosing the central wavelength. With the dual-band LC-OCT prototype reported in this paper, we have been able to obtain images with an unprecedented resolution-to-penetration ratio.

Greyscale fusion was performed to produce images benefiting from the high resolution of the VIS/nIR band and the deep penetration of the nIR band. The “up-down” fusion method requires that the penetration is uniform along the width of the images, which is not always the case. For example, a black hair at the surface of the skin could absorb light strongly in the VIS/nIR band and little in the nIR band. Indeed, black hairs are concentrated in melanin whose absorption spectrum extends to the near infrared part of the spectrum but decreases rapidly with wavelength [25]. In that case, the VIS/nIR could be absorbed locally near the surface of the skin but the columns of the image without signal in the VIS/nIR band would still appear in the compounded image using the “up-down” method. However, the greyscale fusion has more of a visual purpose, highlighting differences between the two bands would be the role of color fusion.

Color representation could be a valuable tool for contrast enhancement and for highlighting spectroscopic differences of the sample between the two bands. It may possible to add a band at lower wavelengths, between 500 nm and 700 nm typically [26], even though the penetration depth would be rather low. Also, interpretation of the color images can be delicate, especially in depth. Indeed, the spectral response of the backscattered signal is strongly affected by the absorption and scattering properties of the layers of tissues crossed by the illumination beam, which is the reason why, for example, a red shift naturally occurs in biological samples [27]. This phenomenon needs to be kept in mind when interpreting the images. The high-frequency details in the images appear quite differently in the two bands due to differences in spatial resolution. To avoid misinterpretation due to this effect, the images are smoothed so that they display approximately equal spatial resolutions, which are degraded at least to the resolution of the nIR band.

A spectral band around 1600 nm could have been chosen to produce images with even deeper penetration [28]. However, in our design the maximal imaging depth was limited by the range of amplitude of 800 µm of the piezoelectric stage, which is corresponds to the penetration depth achieved in the 1250-nm spectral band. Besides, working at higher wavelengths would have further degraded the spatial resolution and would have made the comparison between the two bands more difficult. Finally, using two distant spectral bands would have probably required the use of reflective objectives and made the use of immersion media more difficult.

REFERENCES

[1] D. Huang, E.A. Swanson, C.P. Lin, J.S. Schuman, W.G. Stinson, W. Chang, M.R. Hee, T. Flotte, K. Gregory, C. A. Puliafito, and J.G. Fujimoto, "Optical coherence tomography," Science 254, 1178-1181 (1991).

[2] A.M. Zysk, F.T. Nguyen, A.L. Oldenburg, D.L. Marks, and S.A. Boppart, "Optical coherence tomography: a review of clinical development from bench to bedside," J. Biomed. Opt. 12, 051403 (2007).

[3] J.S. Schuman, C.A. Puliafito, J.G. Fujimoto, and J.S. Duker, Optical Coherence Tomography of Ocular Diseases, 3rd ed. (Slack Inc., Thorofare, NJ, 2013).

[4] H.G. Bezerra, M.A. Costa, G. Guagliumi, A.M. Rollins, and D.I. Simon, "Intracoronary optical coherence tomography: A Comprehensive Review," JACC: Cardiovascular Interventions 2, 1035-1046 (2009).

[5] D.C. Adler, Y. Chen, R. Huber, J. Schmitt, J. Connolly, and J.G. Fujimoto, "Three-dimensional endomicroscopy using optical coherence tomography," Nature Photonics 1, 709-716 (2007).

[6] A. Levine, K. Wang, and O. Markowitz, "Optical Coherence Tomography in the Diagnosis of Skin Cancer," Dermatol. Clinics 35, 465-488 (2017).

[7] A. Dubois, O. Levecq, H. Azimani, D. Siret, A. Barut, M. Suppa, V. Del Marmol, J. Malvehy, E. Cinotti, J.L. Perrot, "Line-field confocal optical coherence tomography for in situ diagnosis of skin tumors," J. Biomed. Opt. 23, 106007 (2018).
[8] W. Drexler, U. Morgner, F. Kärtner, C. Pitris, S. Boppart, X. Li, E. Ippen, and J.G. Fujimoto, "In vivo ultrahigh-resolution optical coherence tomography," Opt. Lett. 24, 1221-1223 (1999).
[9] G. Humbert, W.J. Wadsworth, S.G. Leon-Saval, J.C. Knight, T.A. Birks, P.St.J. Russell, M.J. Lederer, D. Kopf, K. Wiesauer, E.I. Breuer, and D. Stifter, "Supercontinuum generation system for optical coherence tomography based on tapered photonic crystal fibre," Opt. Express 14, 1596-1603 (2006).
[10] Y. Chen, S.-W. Huang, A. D. Aguirre, and J. G. Fujimoto, "High-resolution line-scanning optical coherence microscopy," Opt. Lett. 32, 1971-1973 (2007).
[11] A. Dubois, O. Levecq, H. Azimani, A. Davis, J. Ogien, D. Siret, and A. Barut, "Line-field confocal time-domain optical coherence tomography with dynamic focusing," Opt. Express 26, 33534-33542 (2018).
[12] J.M. Schmitt, A. Knuttel, M. Yadlowsky, and M.A. Eckhaus,"Optical coherence tomography of a dense tissue: statistics of attenuation and backscattering," Phys. Med. Biol. 39, 1705-1720 (1994).
[13] S.H. Tseng, P. Bargo, A. Durkin, and N. Kollias, "Chromophore concentrations, absorption and scattering properties of human skin in-vivo," Opt. Express 17, 14599-14617 (2009).
[14] A. Alex, B. Povazay, B. Hofer, S. Popov, C. Glittenberg, S. Binder, W. Drexler, "Multispectral in vivo three-dimensional optical coherence tomography of human skin," J. Biomed. Opt. 15, 026025 (2010).
[15] F. Spöler, S. Kray, P. Grychtol, B. Hermes, J. Bornemann, M. Först, and H. Kurz, "Simultaneous dual-band ultra-high resolution optical coherence tomography," Opt. Express 15, 10832-10841 (2007).
[16] D. Sacchet, J. Moreau, P. Georges, and A. Dubois, "Simultaneous dual-band ultra-high resolution full-field optical coherence tomography," Opt. Express 16, 19434-19446 (2008).
[17] P. Cimalla, J. Walther, M. Mehner, M. Cuevas, and E. Koch, "Simultaneous dual-band optical coherence tomography in the spectral domain for high resolution in vivo imaging," Opt. Express 17, 19486-19500 (2009).
[18] A. Federici and A. Dubois, "Three-band, 1.9-μm axial resolution full-field optical coherence microscopy over a 530–1700 nm wavelength range using a single camera," Opt. Lett. 39, 1374-1377 (2014).
[19] A. Dubois, "Focus defect and dispersion mismatch in full-field optical coherence microscopy," Appl. Opt. 56, D142-D150 (2017).
[20] K.G. Larkin, "Efficient nonlinear algorithm for envelope detection in white light interferometry," J. Opt. Soc. Am. A 13, 832-843 (1996).
[21] G. Gianto, F. Salzenstein, and P. Montgomery, "Comparison of envelope detection techniques in coherence scanning interferometry," Appl. Opt. 55, 6763-6774 (2016).
[22] W.Y. Oh, B. E. Bouma, N. Iftimia, S. H. Yun, R. Yelin, and G. J. Tearney, "Ultrahigh-resolution full-field optical coherence microscopy using InGaAs camera," Opt. Express 14, 726-735 (2006).
[23] C. Magnain, H. Wang, S. Sakadžić, B. Fischl, and D.A. Boas, "En face speckle reduction in optical coherence microscopy by frequency compounding," Opt. Lett. 41, 1925-1928 (2016).
[24] J.M. Schmitt, S.H. Xiang, and K.M. Yung, "Speckle in optical coherence tomography," J. Biomed. Opt. 4, 95-105 (1999).
[25] M.L. Tran, B. J. Powell, and P. Meredith, "Chemical and Structural Disorder in Eumelanins: A Possible Explanation for Broadband Absorbance," Biophys. J. 90, 743-752 (2006).
[26] X. Shu X, L. Beckmann L, H. Zhang, "Visible-light optical coherence tomography: a review," J. Biomed. Opt. 22, 1-14 (2017).
[27] U. Morgner, W. Drexler, F.X. Kärtner, X.D. Li, C. Pitris, E.P. Ippen, and J.G. Fujimoto, "Spectroscopic optical coherence tomography," Opt. Lett. 25, 111-113 (2000).
[28] V.M. Kodach, J. Kalkman, D.J. Faber, and T.G. van Leeuwen, "Quantitative comparison of the OCT imaging depth at 1300 nm and 1600 nm," Biomed. Opt. Express 1, 176-185 (2010).